

http://pubs.acs.org/journal/aelccp

# Organic Semiconducting Ligands Passivated CsPbBr<sub>3</sub> Nanoplatelets for Blue Light-Emitting Diodes

He Liu, Tunde Blessed Shonde, Oluwadara Joshua Olasupo, Md Sazedul Islam, Tarannuma Ferdous Manny, Maxim Woodhouse, Xinsong Lin, J. S. Raaj Vellore Winfred, Keyou Sam Mao, Eric Lochner, Iqra Fatima, Kenneth Hanson, and Biwu Ma\*

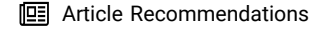


Cite This: ACS Energy Lett. 2023, 8, 4259-4266



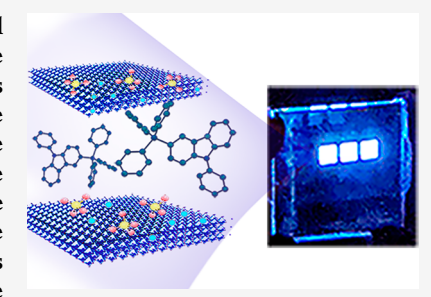
**ACCESS** I

III Metrics & More



s Supporting Information

ABSTRACT: Metal halide perovskite nanocrystals have shown tremendous potential for application in light-emitting diodes (LEDs) due to their unique and remarkable optoelectronic properties. Here, we report the development of CsPbBr<sub>3</sub> nanoplatelets (NPLs) with surface passivation by organic semiconducting ligands for blue LEDs. The use of two organic salts, triphenyl (9-phenyl-9H-carbazol-3-yl) phosphonium sulfate (TPPcarz<sub>2</sub>SO<sub>4</sub>) and triphenyl (9-phenyl-9H-carbazol-3-yl) phosphonium bromide (TPPcarzBr), as surface treatment agents allows for the preparation of 300 nm size CsPbBr<sub>3</sub> NPLs with a blue emission peaked at 455 nm and a photoluminescence quantum efficiency (PLQE) of 82%. Moreover, the charge-transporting TPPcarz<sup>+</sup> units improve the conductivity of thin films based on CsPbBr<sub>3</sub> NPLs and the band edge alignments for blue LEDs. As a result, blue LEDs based on these CsPbBr<sub>3</sub> NPLs exhibit



high external quantum efficiencies (EQEs) of up to 4.15%, a maximum luminance of 1511 cd m<sup>-2</sup>, and a half-lifetime of 50 min (at 100 cd/cm<sup>2</sup>).

etal halide perovskites have attracted tremendous interest as next-generation light-emitting materials for their remarkable optical properties, including narrow band emissions with low full width at half maximum (fwhm), up to near-unity photoluminescence quantum efficiencies (PLQEs), and exceptional color tunability covering the whole visible spectral region from deep blue to the nearinfrared.<sup>1,2</sup> Electroluminescence devices or light-emitting diodes (LEDs) based on metal halide perovskites (PeLEDs) have been heavily investigated as an alternative LED technology in recent years with their external quantum efficiencies (EQEs) approaching those of organic and quantum dot-based LEDs.3-5 Like existing LED technologies, achieving efficient and stable blue PeLEDs is one of the most challenging tasks. To date, the overall performance of blue PeLEDs is far behind those of near-infrared, red, and green ones. 6-1

To achieve blue PeLEDs, strategies involving synthetic control of composition and dimensionality of metal halide perovskites have been developed over the past few years for the preparation of blue-emitting perovskite layers. For instance, mixed halide perovskites containing controlled ratios of Br and Cl can exhibit blue emission with highly tuned peak wavelengths. However, the spectral instability of mixed halide perovskites is inevitable due to ion migration and phase segregation under electrical fields. Reducing the dimension-

ality with the realization of quantum size effects on metal halide perovskites represents another effective method for color tuning. Quantum confined metal halide perovskite nanocrystals (NCs), such as 2D nanoplatelets (NPLs) and 0D quantum dots, as well as quasi-2D perovskites have been developed for the fabrication of blue PeLEDs, which exhibit significantly better spectral stability than those based on mixed halide perovskites. Pecently, we reported a facile synthetic approach for the preparation of blue-emitting CsPbBr<sub>3</sub> NPLs with treatment by an organic sulfate, 2,2-(ethylenedioxy) bis(ethylammonium) sulfate (EDBESO<sub>4</sub>), which exhibit remarkably enhanced PLQE (85%) and stability as compared to pristine CsPbBr<sub>3</sub> NPLs (PLQE of 28%) coated with oleylammonium. Using EDBESO<sub>4</sub>-treated CsPbBr<sub>3</sub> NPLs as emitters, we have demonstrated blue PeLEDs with excellent spectral stability. However, the inferior charge injection and

Received: August 1, 2023 Accepted: September 14, 2023



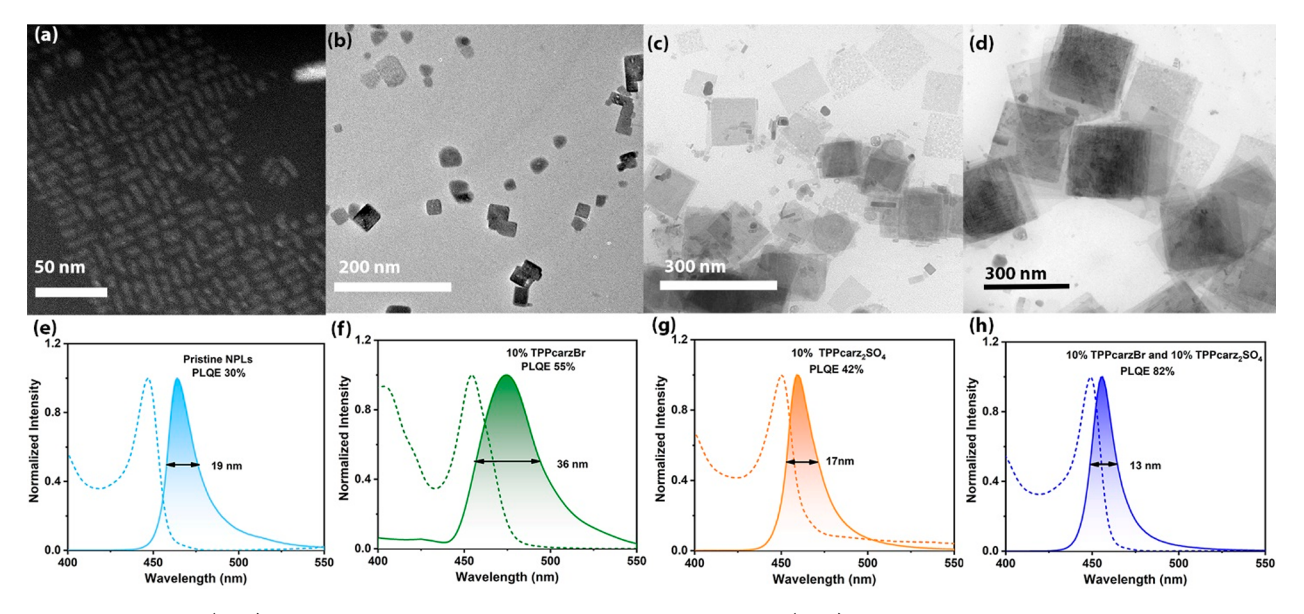


Figure 1. TEM images (a-d) and corresponding absorption and emission spectra (e-h) of  $CsPbBr_3$  nanocrystals obtained with different ratios of the capping ligands: (a and e) without any  $TPPcarz_2F$  or  $TPPcarz_2SO_4$ ; (b and f)  $TPPcarz_2F$ /oleylamine = 0.1:1; (c and g)  $TPPcarz_2SO_4$ /oleylamine = 0.1:1; (d and h)  $TPPcarz_2F$ / $TPPcarz_2SO_4$ /oleylamine = 0.1:0.1:1.

transport in these blue PeLEDs have limited the device performance with EQEs of less than 2%.

In this work, we have developed large size CsPbBr<sub>3</sub> NPLs with surface passivation by organic semiconducting ligands in addition to oleylammonium to address charge injection and transport issues. By using triphenyl (9-phenyl-9H-carbazol-3yl) phosphonium sulfate (TPPcarz<sub>2</sub>SO<sub>4</sub>) and triphenyl (9phenyl-9H-carbazol-3-yl) phosphonium bromide (TPPcarzBr) for surface treatment, CsPbBr<sub>3</sub> NPLs with a thickness of 3 units of PbBr<sub>6</sub><sup>4-</sup> octahedra (around 2 nm) and lateral size of up to 300 nm have been synthesized for the first time. Solution-processed thin films based on TPPcarz<sub>2</sub>SO<sub>4</sub> and TPPcarzBr treated CsPbBr3 NPLs exhibit a narrow band blue emission peaked at 455 nm with PLQEs of up to 82% and good stability. More importantly, TPPcarz<sup>+</sup>, as an energetically aligned conductive ligand, has enabled improvement of charge mobility by orders of magnitude, which prevented charge accumulation with balanced charge injection at the interfaces, circumventing the key bottleneck of low efficiency and inferior stability of PeLEDs based on CsPbBr<sub>3</sub> NPLs. When employing these large size CsPbBr3 NPLs in PeLEDs, a maximum luminance of 1511 cd m<sup>-2</sup> and an EQE of 4.15% were achieved, respectively, which are the best values reported to date for pure blue PeLEDs based on CsPbBr3 NPLs.

Several colloidal synthesis methods have been reported for the preparation of blue-emitting CsPbBr<sub>3</sub> NPLs, including ligand-assisted reprecipitation, hot-injection synthesis, and ligand-assisted ultrasonication. To the best of our knowledge, most blue-emitting CsPbBr<sub>3</sub> NPLs developed to date have small sizes of tens of nanometers wide and are surface passivated by insulating organic ligands, which are not ideal for their applications in optoelectronic devices. Replacing insulating organic ligands with conjugated and conductive ligands to improve charge transport properties has been demonstrated for perovskite NCs with green and red emissions, but not blue-emitting NPLs. The main challenges of producing blue-emitting CsPbBr<sub>3</sub> NPLs passivated by organic semiconducting ligands are twofold: (i) The quantized emission and fusion issue of anisotropic

CsPbBr<sub>3</sub> NPLs make it difficult to modulate their surface environments without affecting their optical properties. (ii) For the large bandgap of CsPbBr<sub>3</sub> NPLs with a deep valence band, it is not trivial to identify surface passivation ligands with appropriate band structures.<sup>24</sup> Based on our previous work,<sup>25,26</sup> we investigated the potential of two organic semiconducting salts, TPPcarz<sub>2</sub>SO<sub>4</sub> and TPPcarzBr, as surface passivation agents for blue-emitting CsPbBr<sub>3</sub> NPLs. New CsPbBr<sub>3</sub> NPLs were synthesized following a modified method with TPPcarz<sub>2</sub>SO<sub>4</sub> and TPPcarzBr mixing with insulating oleylamine, which was used to induce directional growth and form dimensional confinement of CsPbBr<sub>3</sub> NPLs.<sup>27,28</sup> Detailed synthetic procedures can be found in the Supporting Information.

To minimize the amount of insulating oleylammonium cations on the surfaces of CsPbBr<sub>3</sub> NPLs, while maintaining the uniform thicknesses of NPLs, the amounts of TPPcarz<sub>2</sub>SO<sub>4</sub> and TPPcarzBr were delicately modulated by changing their feed molar ratios to oleylamine in the precursor solutions. Figure 1 shows the transmission electron microscopy (TEM) images of CsPbBr<sub>3</sub> NPLs prepared by using different synthetic conditions and their corresponding optical properties. Rectangle-shaped CsPbBr<sub>3</sub> NPLs with a lateral size of 5-20 nm were obtained using a reported method without the addition of any TPPcarzBr or TPPcarz2SO4 (hereafter referred to as pristine CsPbBr<sub>3</sub> NPLs as shown in Figure 1a).<sup>27,28</sup> As expected, pristine CsPbBr<sub>3</sub> NPLs exhibit a blue emission peaked at 465 nm with an fwhm of 19 nm and a PLQE of 30% (Figure 1e). The other three CsPbBr<sub>3</sub> NPLs were obtained by adding 10% TPPcarzBr, 10% TPPcarz2SO4, and 10% TPPcarzBr/10% TPPcarz<sub>2</sub>SO<sub>4</sub> to the precursor solutions. For the case of adding 10% TPPcarzBr, nonuniform CsPbBr<sub>3</sub> NPLs with larger sizes were obtained (Figure 1b), which exhibit a red-shifted and broadened blue emission peaked at 475 nm with an fwhm of 36 nm and a PLQE of 55% (Figure 1f), as a result of reduced extent of quantum confinement. For the case of adding 10% TPPcarz<sub>2</sub>SO<sub>4</sub>, CsPbBr<sub>3</sub> NPLs with large lateral sizes of around 130 nm were obtained (Figure 1c), suggesting that  $SO_4^{\ 2-}$  can increase the Ostwald ripening process. As

ACS Energy Letters http://pubs.acs.org/journal/aelccp Letter

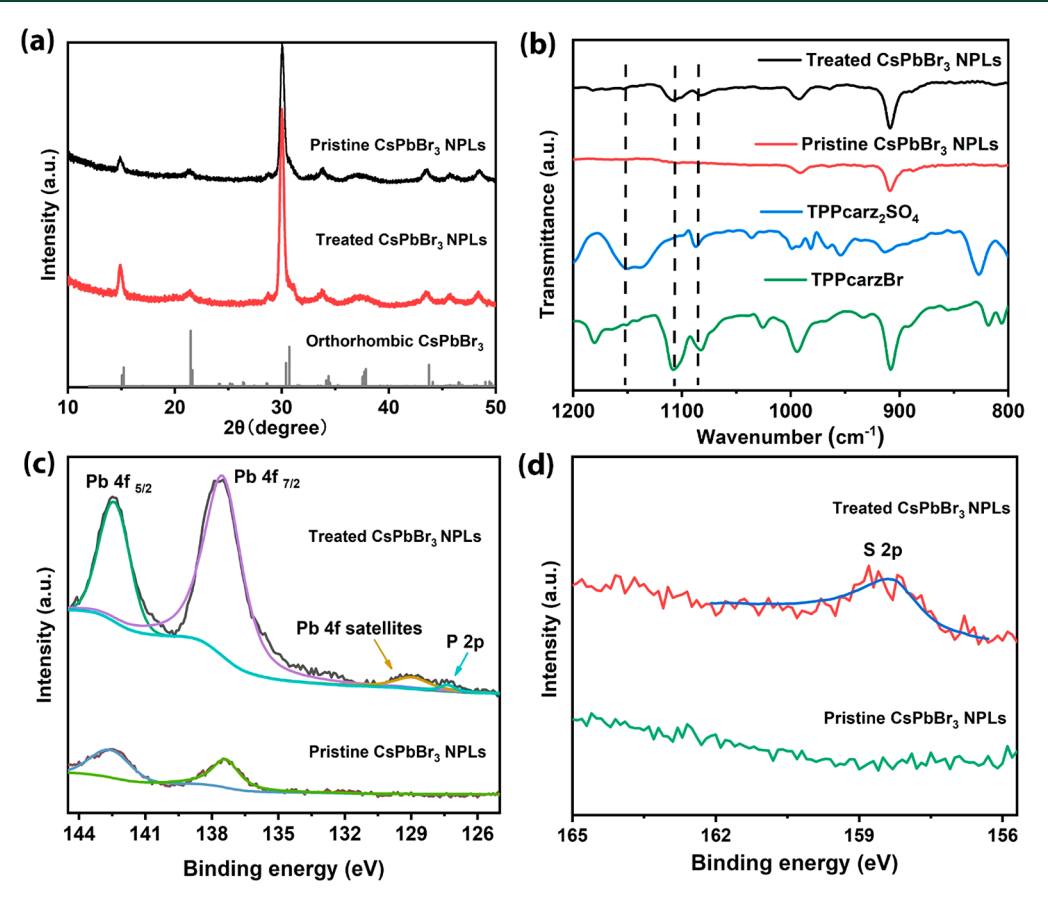


Figure 2. (a) XRD patterns of pristine CsPbBr<sub>3</sub> NPLs and treated CsPbBr<sub>3</sub> NPLs. The reference for orthorhombic CsPbBr<sub>3</sub> is PDF Card No. 01-085-6500. (b) FTIR spectra of treated CsPbBr<sub>3</sub> NPLs, pristine CsPbBr<sub>3</sub> NPLs, TPPcarzBr, and TPPcarz<sub>2</sub>SO<sub>4</sub>. (c) XPS spectra corresponding to Pb 4f and P 2p of treated CsPbBr<sub>3</sub> NPLs and pristine CsPbBr<sub>3</sub> NPLs. (d) XPS spectra of S 2p for treated CsPbBr<sub>3</sub> NPLs and pristine CsPbBr<sub>3</sub> NPLs.

compared to the pristine CsPbBr<sub>3</sub> NPLs, CsPbBr<sub>3</sub> NPLs prepared with the addition of 10% TPPcarz<sub>2</sub>SO<sub>4</sub> exhibit a similar blue emission with a smaller fwhm of 17 nm and a higher PLQE of 42%. Finally, for the case of adding both 10% TPPcarzBr and 10% TPPcarz<sub>2</sub>SO<sub>4</sub>, highly uniform CsPbBr<sub>3</sub> NPLs with the largest lateral sizes of up to 300 nm were obtained (Figures 1d and S1). A blue emission peaked at 455 nm (a thickness of 3 units of PbBr<sub>6</sub><sup>4-</sup> octahedra around 2 nm) with a high PLQE of 82% and a remarkably low fwhm of 13 nm is achieved for these CsPbBr<sub>3</sub> NPLs.<sup>19</sup> The corresponding spectral curves for the calculation of PLQEs are shown in Figure S2.

The effects of the addition of both TPPcarzBr and TPPcarz<sub>2</sub>SO<sub>4</sub> on the morphological and photophysical properties of CsPbBr<sub>3</sub> NPLs are multifold. First, for the bulkiness and unique charge distribution, TPPcarz<sup>+</sup> can provide steric or electrostatic stabilization to increase the lateral size of the CsPbBr<sub>3</sub> NPLs. The similar way of tuning the lateral size of perovskite NPLs by varying the ratio of short and long ligands has been reported previously.<sup>29</sup> Second, SO<sub>4</sub><sup>2-</sup> can bind uncoordinated Pb<sup>2+</sup> to passivate the surface defects and suppress the coalescence of CsPbBr<sub>3</sub> NPLs.<sup>30</sup> Third, the presence of Br<sup>-</sup> from TPPcarzBr could reduce Br<sup>-</sup> vacancies on CsPbBr<sub>3</sub> NPLs, resulting in enhanced PLQEs.<sup>20</sup> Provided that CsPbBr<sub>3</sub> NPLs treated by both TPPcarzBr and TPPcarz<sub>2</sub>SO<sub>4</sub> exhibit the desired structural and optical properties, we have focused on them (referred to as treated

CsPbBr<sub>3</sub> NPLs) for more detailed studies and used them for the fabrication of pure blue PeLEDs.

To confirm the composition and structure of treated CsPbBr<sub>3</sub> NPLs, powder X-ray diffraction (PXRD) was performed with the results shown in Figure 2a. The structures of both pristine and treated CsPbBr<sub>3</sub> NPLs are assigned to the Phnm space group, corresponding to orthorhombic CsPbBr<sub>3</sub> (PDF# 01-085-6500). The treated and pristine NPLs have the tendency to self-assemble into stacked superlattices on the substrate, as evidenced by the periodic diffraction shown in the small-angle X-ray scattering pattern (Figure S3). The distance (d-spacing) between organic ligand layers within the stacking NPLs was calculated to be around 27 Å ( $2\theta = 3.3^{\circ}$ ), which agrees well with the previously reported value.<sup>31</sup> Fourier transform infrared (FTIR) spectroscopy and X-ray photoelectron spectroscopy (XPS) measurements were performed to verify the presence of multiple ions (TPPcarz+, SO<sub>4</sub>2-, and Br<sup>-</sup>) on the surfaces of the CsPbBr<sub>3</sub> NPLs. As shown in Figure 2b, the vibration peaks at 1107 and 1082  $cm^{-1}$  for the phenyl groups in TPPcarz<sup>+</sup> are detected in treated CsPbBr<sub>3</sub> NPLs, confirming the interactions between TPPcarz<sup>+</sup> and CsPbBr<sub>2</sub> NPLs. The characteristic broad peak at around 1150 cm<sup>-1</sup>, attributed to the triply degenerate v<sub>3</sub> band of SO<sub>4</sub><sup>2-</sup>, could also be found in purified treated CsPbBr<sub>3</sub> NPLs. XPS measurements were performed on thin films based on purified pristine and treated CsPbBr3 NPLs to reveal the changes of the surface state with the addition of two organic salts (Figure 2c,d). A higher intensity of the Pb 4f peak was recorded for treated

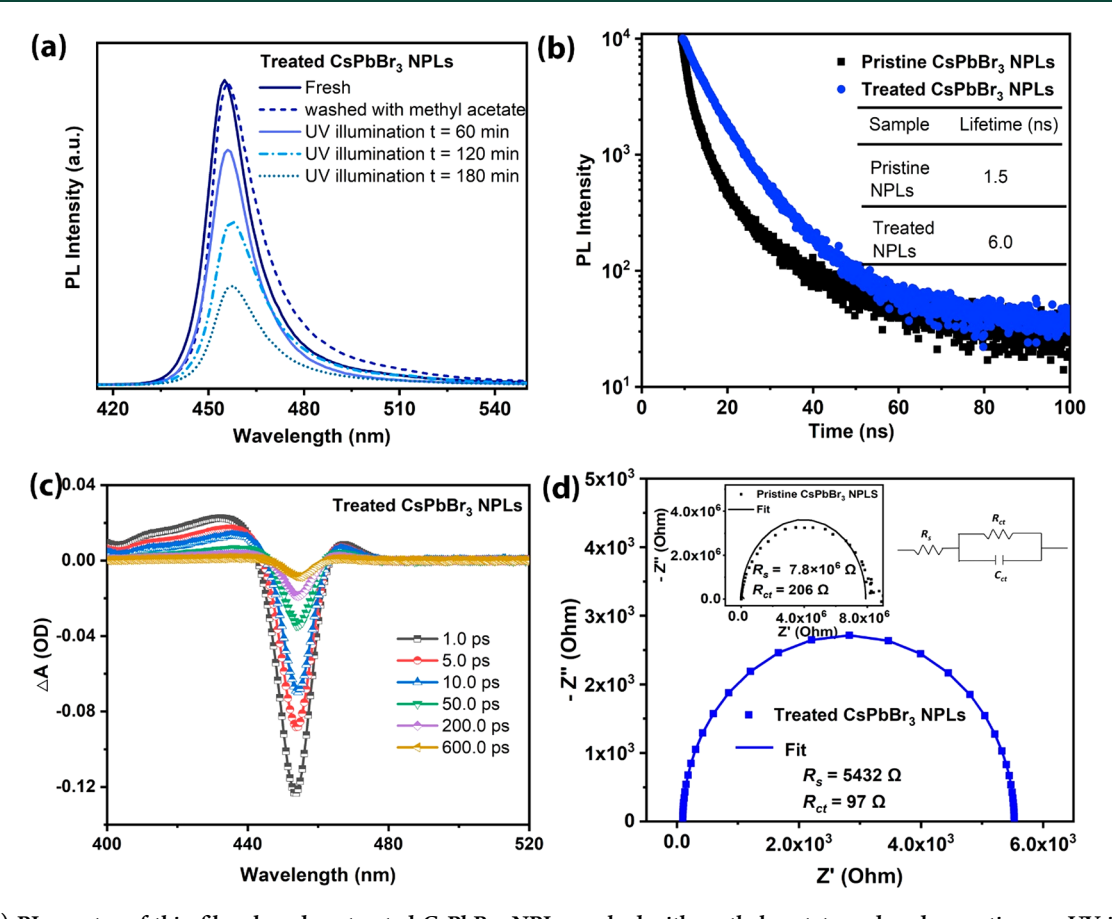


Figure 3. (a) PL spectra of thin films based on treated CsPbBr<sub>3</sub> NPLs washed with methyl acetate and under continuous UV illumination. (b) Time-resolved PL decay curves and lifetimes of pristine CsPbBr<sub>3</sub> NPLs and treated CsPbBr<sub>3</sub> NPLs. (c) TA spectra of treated CsPbBr<sub>3</sub> NPLs recorded at different pump—probe decay times with the excitation wavelength of 380 nm. (d) Nyquist plots of devices based on treated CsPbBr<sub>3</sub> NPLs (inset shows Nyquist plots of devices based on pristine CsPbBr<sub>3</sub> NPLs).

CsPbBr<sub>3</sub> NPLs than for pristine CsPbBr<sub>3</sub> NPLs, which is likely due to the less insulating organic ligands on the surfaces. In treated CsPbBr<sub>3</sub> NPLs, the features of phosphorus (127.3 eV) in the P 2p spectrum region confirm the presence of TPPcarz<sup>+</sup>. The high conductivity of TPPcarz+ causes the changes of electronic and chemical environments for Pb2+ with a Pb 4f satellite peak appearing at a binding energy 128.9 eV.<sup>32</sup> The changes of surrounding environments for Pb2+ are also evidenced by the narrower Pb 4f peak in treated CsPbBr<sub>3</sub> NPLs, as a result of fewer Pb-oleate interactions in treated CsPbBr<sub>3</sub> NPLs than in pristine CsPbBr<sub>3</sub> NPLs.<sup>20</sup> The appearance of sulfur in the S 2p spectrum at 158.3 eV provides strong evidence for the existence of  $\mathrm{SO_4}^{2-}$  in treated CsPbBr<sub>3</sub> NPLs. The accurate elemental composition of treated CsPbBr<sub>3</sub> NPLs was quantified by X-ray fluorescence (XRF). XRF spectra of P and S collected from the purified treated CsPbBr<sub>3</sub> NPLs were shown in Figure S4a,b. From the corresponding calibration curves of P5+, S6+, Cs+, Pb2+, and Br (Figure S5), the quantitative molar ratio of these elements was determined as P: S: Cs: Pb: Br = 0.22:0.20:0.46:1:4.26. The ratio values obtained for pristine CsPbBr<sub>3</sub> NPLs were Cs: Pb: Br = 0.61:1:3.79.<sup>33</sup> The XRF results further confirm the surface passivation of CsPbBr<sub>3</sub> NPLs by TPPcarz<sup>+</sup>, SO<sub>4</sub><sup>2-</sup>, and Br<sup>-</sup>, which are stable after the purification process.

To utilize synthesized CsPbBr<sub>3</sub> NPLs for solid-state electronic devices, it is essential to obtain thin films with sufficient uniformity and smoothness. Spin coating of CsPbBr<sub>3</sub> NPL solutions in octane was carried out to prepare thin films

on cleaned glass substrates (details in Experimental Section in the Supporting Information). Atomic force microscopy (AFM) was used to characterize the morphology of spun cast thin films, with results shown in Figure S6. Thin films based on pristine CsPbBr<sub>3</sub> NPL show rough and uneven coverage with a root-mean-square roughness  $R_q$  of 1.89 nm, which is likely due to the dissociation of surface ligands and accumulation of NPLs. In contrast, thin films based on treated CsPbBr<sub>3</sub> NPLs are more uniform and smooth with an  $R_a$  of 0.21 nm, which is attributed to the relatively high viscosity of the treated CsPbBr3 NPL solution and excellent stable dispersion of CsPbBr<sub>3</sub> NPLs.<sup>25</sup> The optoelectronic properties and stability of thin films based on treated CsPbBr3 NPLs were also fully characterized. As shown in Figure 3a, thin films based on treated CsPbBr3 NPLs before and after washing with antisolvent exhibit almost the same emission spectra, suggesting that treatment by TPPcarzBr and TPPcarz2SO4 can reduce defect sites and avoid coalescence of NPLs during the purification and spin-coating process. The PLQEs of thin films based on treated CsPbBr3 NPLs were determined to be up to 82%. The photostability of thin films based on treated CsPbBr<sub>3</sub> NPLs was tested under continuous UV irradiation (365 nm, 40 mW/cm<sup>2</sup>), which shows only a small intensity reduction after 60 min and no shift in the emission peak after 180 min (Figure 3a). In contrast, thin films based on pristine CsPbBr3 NPLs exhibit much lower PLQEs with additional redshifted emission peaks, as a result of the formation of surface defects and coalescence due to the loss of highly dynamic

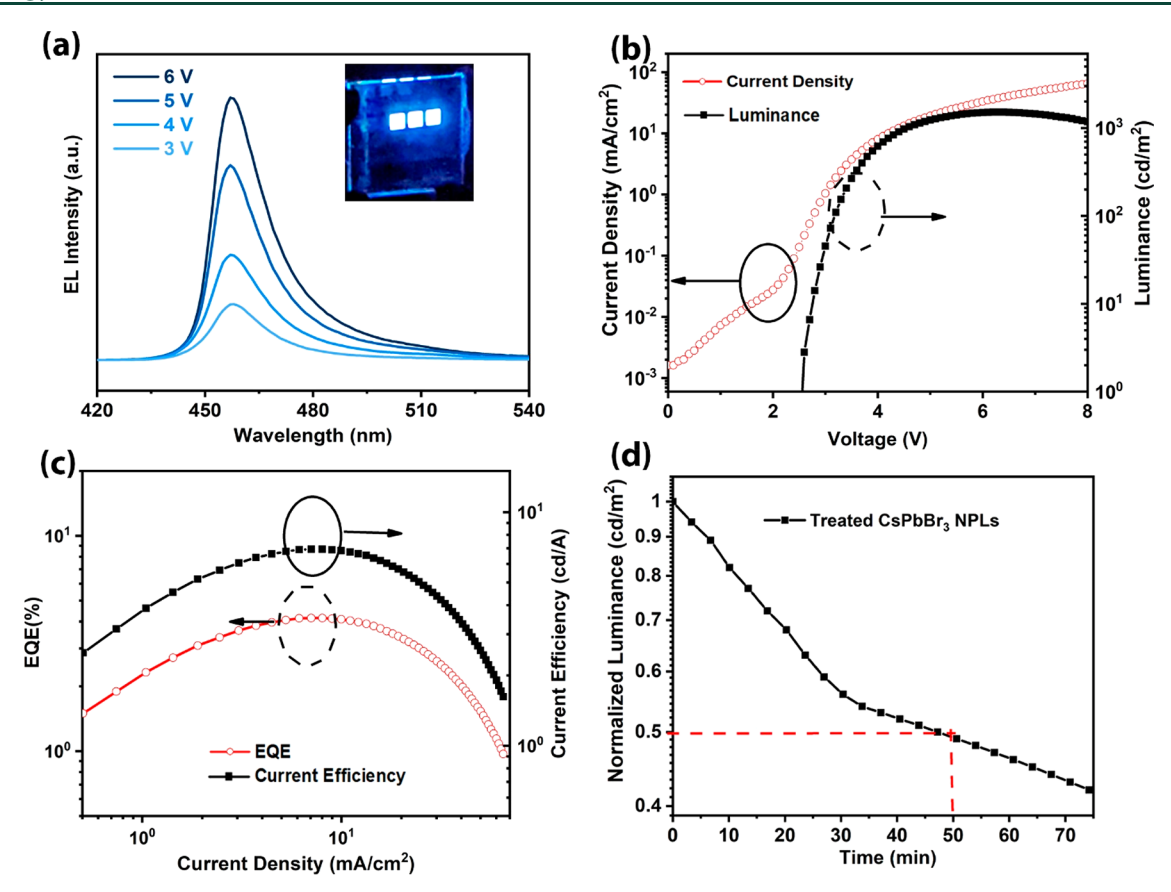


Figure 4. (a) EL spectra at different bias voltages for the device based on treated CsPbBr<sub>3</sub> NPLs. (b) Current density-voltage-luminance (J-V-L) plots for the device based on treated CsPbBr<sub>3</sub> NPLs. (c) EQE-current density-current efficiency plots for the device based on treated CsPbBr<sub>3</sub> NPLs. (d) Half-lifetime  $(T_{50})$  of PeLEDs based on treated CsPbBr<sub>3</sub> NPLs at an initial luminance of ~100 cd m<sup>-2</sup>.

oleylammonium ligands during the purification process (Figure S7a).  $^{34}$ 

Time-resolved PL decay curves for thin films based on pristine and treated CsPbBr<sub>3</sub> NPLs are shown in Figure 3b. A longer PL decay lifetime of 6.0 ns was recorded for thin films based on treated CsPbBr<sub>3</sub> NPLs relative to the pristine CsPbBr<sub>3</sub> NPLs (1.5 ns), presumably due to nonradiative recombination pathways through surface defects being suppressed by treatment with two organic salts. The low density of surface defects can be further validated by a small Urbach tail for the thin films based on treated CsPbBr<sub>3</sub> NPLs.<sup>20,35</sup> A smaller Urbach energy of 15 meV was recorded for thin films based on treated CsPbBr3 NPLs than that of thin films based on pristine CsPbBr<sub>3</sub> NPLs of 41 meV (Figure S7b). Transient absorption (TA) measurements were conducted to further reveal the ultrafast exciton dynamic processes in thin films based on treated and pristine CsPbBr<sub>3</sub> NPLs. Thin films based on treated CsPbBr<sub>3</sub> NPLs are found to exhibit a bleach peak at 455 nm, corresponding to excitons formed in n = 3 metal halide quantum wells (QWs) (Figure 3c).<sup>36</sup> In contrast, multiple bleach peaks at 460-530 nm are shown in thin films based on pristine CsPbBr<sub>3</sub> NPLs (Figure S8a). The redshift of bleach peaks with the delay time indicates a distribution of metal halide QWs with different thicknesses and merging of the NPLs into bulk perovskites during the measurement.

The conductivity of thin films based on treated and pristine CsPbBr<sub>3</sub> NPLs was examined by electrochemical impedance spectroscopy (EIS). Nyquist plots and the parameters of charge transport resistance ( $R_{ct}$ ) and the series resistance ( $R_s$ )

have been characterized using an appropriate equivalent circuit as shown in Figure 3d. Both R<sub>ct</sub> and R<sub>s</sub> decrease significantly for thin films based on treated CsPbBr3 NPLs as compared to those of thin films based on pristine CsPbBr<sub>3</sub> NPLs, from 206 to 97  $\Omega$ , and from 7.8  $\times$  10<sup>6</sup>  $\Omega$  to 5432  $\Omega$ , respectively, indicating a much higher conductivity of thin films based on treated CsPbBr<sub>3</sub> NPLs. Interfacial charge transfer was further investigated by electron-only and hole-only devices via current density-voltage (J-V) traces (Figure S8b). It was found that both electron and hole currents in thin films based on treated CsPbBr<sub>3</sub> NPLs are pronouncedly enhanced compared to those of thin films based on pristine CsPbBr3 NPLs. The charge carrier mobilities of thin films based on treated and pristine CsPbBr<sub>3</sub> NPLs were then measured by using space-chargelimited currents (SCLCs) (Figure S9). Hole and electron mobilities of  $8.7 \times 10^{-5}$  and  $5.9 \times 10^{-5}$  cm<sup>2</sup> V<sup>-1</sup> s<sup>-1</sup> were obtained for thin films based on treated CsPbBr3 NPLs, which are significantly higher than those of thin films based on pristine CsPbBr<sub>3</sub> NPLs  $(1.3 \times 10^{-6} \text{ cm}^2 \text{ V}^{-1} \text{ s}^{-1} \text{ for hole}$  mobility,  $5.1 \times 10^{-6} \text{ cm}^2 \text{ V}^{-1} \text{ s}^{-1}$  for electron mobility). The densities of hole and electron traps of pristine and treated CsPbBr<sub>3</sub> NPLs films can be calculated using the equation  $N_{(e/h)} = (2V_{TFL}\varepsilon_r \varepsilon_0)/(eL^2)$ , where  $N_{(e/h)}$  is the trap density for electron or hole, respectively;  $V_{\mathrm{TFL}}$  is trap-filled limiting voltage, e is the elementary charge, and d is the film thickness;  $\varepsilon_{\rm r}$  and  $\varepsilon_{\rm 0}$  are the dielectric constant and vacuum permittivity, respectively. As expected, the hole and electron trap densities of treated CsPbBr<sub>3</sub> NPL films  $(2.98 \times 10^{17} \text{ and } 1.10 \times 10^{17})$ cm<sup>-3</sup>) are notably lower than those of pristine CsPbBr<sub>3</sub> NPLs

films  $(7.93 \times 10^{17} \text{ and } 5.93 \times 10^{17} \text{ cm}^{-3})$ , which further confirms the effective passivation by TPPcarz<sub>2</sub>SO<sub>4</sub> and TPPcarzBr. In addition to increased conductivity, the introduction of TPPcarz<sup>+</sup> on treated CsPbBr<sub>3</sub> NPLs was found to be beneficial for the energy level alignment to promote charge injection when they are used as emitting layer in blue PeLEDs. The energy level diagram for a simple blue PeLED based on treated CsPbBr<sub>3</sub> NPLs is shown in Figure S11a. The band edge values for TPPcarz<sup>+</sup> were obtained through UV absorption and cyclic voltammetry for TPPcarzBr and TPPcarz<sub>2</sub>SO<sub>4</sub> (Figure S10a,b),<sup>37</sup> while the values for ITO, PEDOT:PSS, poly(TPD), blue CsPbBr<sub>3</sub> NPLs, and TPBi were obtained from the literature.<sup>38</sup> All of these results suggest that bipolar TPPcarz<sup>+</sup> could facilitate the injection and transport of both electrons and holes.

The thin films based on treated CsPbBr<sub>3</sub> NPLs were used as emitting layer to fabricate blue PeLEDs composed of ITO/ poly(ethylenedioxythiophene): polystyrenesulfonate (PEDOT: PSS)/poly(N, N'-bis(4-butylphenyl)-N,N'-bisphenylbenzidine) (poly-TPD)/CsPbBr<sub>3</sub> NPLs/1,3,5-Tris (1-phenyl-1Hbenzimidazol-2-yl) benzene (TPBi)/LiF/Al. The electroluminescence (EL) spectra with an emission peak at 455 nm at different voltages are shown in Figure 4a. A low turn-on voltage (~2.6 V) is achieved, likely due to the superior conductivity of thin films based on treated CsPbBr3 NPLs. The champion devices produce an EQE of 4.15%, a maximum luminance of 1511 cd m<sup>-2</sup>, and a current efficiency of 8.2 cd A<sup>-1</sup> at 6.3 V (Figure 4b and c), the highest values achieved for blue PeLEDs based on CsPbBr3 NPLs to date. The EQE histogram of 30 devices is shown in Figure S11b, suggesting the excellent reproducibility of these devices with an average EQE of 3.9%. Moreover, the device shows a  $T_{50}$  lifetime of 50 min, which is 2.5 times longer than that of the recent best PeLEDs based on NPLs (Figure 4d).<sup>33</sup> Table S1 summarizes the performance parameters of devices based on the pristine, TPPcarz<sub>2</sub>SO<sub>4</sub>, and TPPcarzBr treated NPLs for comparison.

In summary, we have developed large size CsPbBr<sub>3</sub> NPLs passivated by a combination of three ions of TPPcarz<sup>+</sup>, SO<sub>4</sub><sup>2-</sup>, and Br<sup>-</sup> for the first time. The treated large size CsPbBr<sub>3</sub> NPLs exhibit significantly improved optical and electronic properties compared to conventional small size CsPbBr<sub>3</sub> NPLs passivated only by long alkyl chain insulating ligands. Narrow blue emission peaked at 455 nm with a fwhm of 13 nm and a PLQE of 82% is achieved for these large CsPbBr<sub>3</sub> NPLs, presumably due to their high uniformity and aspect ratio. Partially replacing long alkyl chain insulating ligands with organic semiconducting ligands for the surface passivation of CsPbBr<sub>3</sub> NPLs also enables efficient charge injection and transport, when they are used as an emitting layer in blue PeLEDs, which exhibit high EQEs of up to 4.15% and a half-lifetime of 50 min (at 100 cd/cm<sup>2</sup>). Our work further emphasizes the importance of surface modification and morphological control of perovskite nanocrystals to achieve desired optoelectronic properties for device applications, which paves a new path toward the realization of their full potential.

# ASSOCIATED CONTENT

# Supporting Information

The Supporting Information is available free of charge at https://pubs.acs.org/doi/10.1021/acsenergylett.3c01576.

Experimental Section: chemicals; preparation of triphenyl (9-phenyl-9H-carbazol-3-yl) phosphonium bromide (TPPcarzBr) and triphenyl (9-phenyl-9H-carbazol-3-yl) phosphonium sulfate (TPPcarz<sub>2</sub>SO<sub>4</sub>); synthesis of pristine and treated CsPbBr<sub>3</sub> NPLs; Ppurification of colloidal NPLs; fabrication and testing of PeLEDs; Materials Characterization: TEM image and the histogram of the NPLs lengths; X-ray fluorescence spectra; AFM images; PL spectra; TA spectra; SCLC measurements; absorption spectra; histogram of maximum EQE measured from 30 devices; half-lifetime of PeLEDs (PDF)

## AUTHOR INFORMATION

# **Corresponding Author**

Biwu Ma — Department of Chemistry and Biochemistry, Florida State University, Tallahassee, Florida 32306, United States; oorcid.org/0000-0003-1573-8019; Email: bma@fsu.edu

### **Authors**

**He Liu** – Department of Chemistry and Biochemistry, Florida State University, Tallahassee, Florida 32306, United States

Tunde Blessed Shonde – Department of Chemistry and Biochemistry, Florida State University, Tallahassee, Florida 32306, United States

Oluwadara Joshua Olasupo – Department of Chemistry and Biochemistry, Florida State University, Tallahassee, Florida 32306, United States

Md Sazedul Islam – Department of Chemistry and Biochemistry, Florida State University, Tallahassee, Florida 32306, United States

Tarannuma Ferdous Manny — Department of Chemistry and Biochemistry, Florida State University, Tallahassee, Florida 32306, United States

Maxim Woodhouse – Department of Chemistry and Biochemistry, Florida State University, Tallahassee, Florida 32306, United States

Xinsong Lin – Department of Chemistry and Biochemistry, Florida State University, Tallahassee, Florida 32306, United States

J. S. Raaj Vellore Winfred – Department of Chemistry and Biochemistry, Florida State University, Tallahassee, Florida 32306, United States

Keyou Sam Mao — Magnet Science and Technology, National High Magnetic Field Laboratory, Tallahassee, Florida 32310, United States

Eric Lochner – Department of Physics, Florida State University, Tallahassee, Florida 32306, United States

Iqra Fatima — Department of Chemistry and Biochemistry, Florida State University, Tallahassee, Florida 32306, United States

Kenneth Hanson — Department of Chemistry and Biochemistry, Florida State University, Tallahassee, Florida 32306, United States; ⊚ orcid.org/0000-0001-7219-7808

Complete contact information is available at: https://pubs.acs.org/10.1021/acsenergylett.3c01576

### Notes

The authors declare no competing financial interest.

### ACKNOWLEDGMENTS

The authors thank the National Science Foundation (ECCS-2210902) for support. A portion of this research used

resources provided by the X-ray Crystallography Center (FSU075000XRAY) and the Materials Characterization Laboratory (FSU075000MAC) at the FSU Department of Chemistry and Biochemistry. TEM work was performed at the National High Magnetic Field Laboratory, which is supported by National Science Foundation Cooperative agreement no. DMR-1644779 and the State of Florida. A spectrometer supported by the National Science Foundation under Grant No. CHE-1919633 was used for Transient Absorption Measurements.

# REFERENCES

- (1) Quan, L. N.; Rand, B. P.; Friend, R. H.; Mhaisalkar, S. G.; Lee, T.-W.; Sargent, E. H. Perovskites for Next-Generation Optical Sources. *Chem. Rev.* **2019**, *119* (12), 7444–7477.
- (2) Tan, Z.-K.; Moghaddam, R. S.; Lai, M. L.; Docampo, P.; Higler, R.; Deschler, F.; Price, M.; Sadhanala, A.; Pazos, L. M.; Credgington, D.; Hanusch, F.; Bein, T.; Snaith, H. J.; Friend, R. H. Bright Light-Emitting Diodes Based on Organometal Halide Perovskite. *Nat. Nanotechnol.* **2014**, *9* (9), 687–692.
- (3) Lin, K.; Xing, J.; Quan, L. N.; de Arquer, F. P. G.; Gong, X.; Lu, J.; Xie, L.; Zhao, W.; Zhang, D.; Yan, C.; Li, W.; Liu, X.; Lu, Y.; Kirman, J.; Sargent, E. H.; Xiong, Q.; Wei, Z. Perovskite Light-Emitting Diodes with External Quantum Efficiency Exceeding 20 per Cent. *Nature* **2018**, *562* (7726), 245–248.
- (4) Cao, Y.; Wang, N.; Tian, H.; Guo, J.; Wei, Y.; Chen, H.; Miao, Y.; Zou, W.; Pan, K.; He, Y.; Cao, H.; Ke, Y.; Xu, M.; Wang, Y.; Yang, M.; Du, K.; Fu, Z.; Kong, D.; Dai, D.; Jin, Y.; Li, G.; Li, H.; Peng, Q.; Wang, J.; Huang, W. Perovskite Light-Emitting Diodes Based on Spontaneously Formed Submicrometre-Scale Structures. *Nature* 2018, 562 (7726), 249–253.
- (5) Kim, Y.-H.; Kim, S.; Kakekhani, A.; Park, J.; Park, J.; Lee, Y.-H.; Xu, H.; Nagane, S.; Wexler, R. B.; Kim, D.-H.; Jo, S. H.; Martínez-Sarti, L.; Tan, P.; Sadhanala, A.; Park, G.-S.; Kim, Y.-W.; Hu, B.; Bolink, H. J.; Yoo, S.; Friend, R. H.; Rappe, A. M.; Lee, T.-W. Comprehensive Defect Suppression in Perovskite Nanocrystals for High-Efficiency Light-Emitting Diodes. *Nat. Photonics* **2021**, *15* (2), 148–155.
- (6) Zhu, L.; Cao, H.; Xue, C.; Zhang, H.; Qin, M.; Wang, J.; Wen, K.; Fu, Z.; Jiang, T.; Xu, L.; Zhang, Y.; Cao, Y.; Tu, C.; Zhang, J.; Liu, D.; Zhang, G.; Kong, D.; Fan, N.; Li, G.; Yi, C.; Peng, Q.; Chang, J.; Lu, X.; Wang, N.; Huang, W.; Wang, J. Unveiling the Additive-Assisted Oriented Growth of Perovskite Crystallite for High Performance Light-Emitting Diodes. *Nat. Commun.* **2021**, *12* (1), 5081
- (7) Wang, Y.-K.; Singh, K.; Li, J.-Y.; Dong, Y.; Wang, X.-Q.; Pina, J. M.; Yu, Y.-J.; Sabatini, R.; Liu, Y.; Ma, D.; Liu, J.; Liu, Z.; Gao, Y.; Voznyy, O.; Ma, W.; Fung, M.-K.; Liao, L.-S.; Sargent, E. H. In Situ Inorganic Ligand Replenishment Enables Bandgap Stability in Mixed-Halide Perovskite Quantum Dot Solids. *Adv. Mater.* **2022**, *34* (21), 2200854
- (8) Liu, Z.; Qiu, W.; Peng, X.; Sun, G.; Liu, X.; Liu, D.; Li, Z.; He, F.; Shen, C.; Gu, Q.; Ma, F.; Yip, H.-L.; Hou, L.; Qi, Z.; Su, S.-J. Perovskite Light-Emitting Diodes with EQE Exceeding 28% through a Synergetic Dual-Additive Strategy for Defect Passivation and Nanostructure Regulation. *Adv. Mater.* 2021, 33 (43), 2103268.
- (9) Jiang, Y.; Sun, C.; Xu, J.; Li, S.; Cui, M.; Fu, X.; Liu, Y.; Liu, Y.; Wan, H.; Wei, K.; Zhou, T.; Zhang, W.; Yang, Y.; Yang, J.; Qin, C.; Gao, S.; Pan, J.; Liu, Y.; Hoogland, S.; Sargent, E. H.; Chen, J.; Yuan, M. Synthesis-on-Substrate of Quantum Dot Solids. *Nature* **2022**, *612* (7941), *679*–684.
- (10) Ren, Z.; Wang, K.; Sun, X. W.; Choy, W. C. H. Strategies Toward Efficient Blue Perovskite Light-Emitting Diodes. *Adv. Funct. Mater.* **2021**, *31* (30), 2100516.
- (11) Knight, A. J.; Herz, L. M. Preventing Phase Segregation in Mixed-Halide Perovskites: A Perspective. *Energy Environ. Sci.* **2020**, 13 (7), 2024–2046.

- (12) Wang, H.; Ye, F.; Sun, J.; Wang, Z.; Zhang, C.; Qian, J.; Zhang, X.; Choy, W. C. H.; Sun, X. W.; Wang, K.; Zhao, W. Efficient CsPbBr3 Nanoplatelet-Based Blue Light-Emitting Diodes Enabled by Engineered Surface Ligands. *ACS Energy Lett.* **2022**, *7* (3), 1137—1145
- (13) Hoye, R. L. Z.; Lai, M.-L.; Anaya, M.; Tong, Y.; Galkowski, K.; Doherty, T.; Li, W.; Huq, T. N.; Mackowski, S.; Polavarapu, L.; Feldmann, J.; MacManus-Driscoll, J. L.; Friend, R. H.; Urban, A. S.; Stranks, S. D. Identifying and Reducing Interfacial Losses to Enhance Color-Pure Electroluminescence in Blue-Emitting Perovskite Nanoplatelet Light-Emitting Diodes. ACS Energy Lett. 2019, 4 (5), 1181–1188
- (14) Cho, J.; Jin, H.; Sellers, D. G.; Watson, D. F.; Son, D. H.; Banerjee, S. Influence of Ligand Shell Ordering on Dimensional Confinement of Cesium Lead Bromide (CsPbBr3) Perovskite Nanoplatelets. *J. Mater. Chem. C* **2017**, *5* (34), 8810–8818.
- (15) Yin, W.; Li, M.; Dong, W.; Luo, Z.; Li, Y.; Qian, J.; Zhang, J.; Zhang, W.; Zhang, Y.; Kershaw, S. V.; Zhang, X.; Zheng, W.; Rogach, A. L. Multidentate Ligand Polyethylenimine Enables Bright Color-Saturated Blue Light-Emitting Diodes Based on CsPbBr3 Nano-platelets. ACS Energy Lett. 2021, 6 (2), 477–484.
- (16) Ghimire, S.; Klinke, C. Two-Dimensional Halide Perovskites: Synthesis, Optoelectronic Properties, Stability, and Applications. *Nanoscale* **2021**, *13* (29), 12394–12422.
- (17) Liu, Y.; Li, Z.; Xu, J.; Dong, Y.; Chen, B.; Park, S. M.; Ma, D.; Lee, S.; Huang, J. E.; Teale, S.; Voznyy, O.; Sargent, E. H. Wide-Bandgap Perovskite Quantum Dots in Perovskite Matrix for Sky-Blue Light-Emitting Diodes. J. Am. Chem. Soc. 2022, 144 (9), 4009–4016.
- (18) Liu, H.; Worku, M.; Mondal, A.; Shonde, T. B.; Chaaban, M.; Ben-Akacha, A.; Lee, S.; Gonzalez, F.; Olasupo, O.; Lin, X.; Vellore Winfred, J. S. R.; Xin, Y.; Lochner, E.; Ma, B. Efficient and Stable Blue Light Emitting Diodes Based on CsPbBr3 Nanoplatelets with Surface Passivation by a Multifunctional Organic Sulfate. *Adv. Energy Mater.* 2023, 13, 2201605.
- (19) Otero-Martínez, C.; Ye, J.; Sung, J.; Pastoriza-Santos, I.; Pérez-Juste, J.; Xia, Z.; Rao, A.; Hoye, R. L. Z.; Polavarapu, L. Colloidal Metal-Halide Perovskite Nanoplatelets: Thickness-Controlled Synthesis, Properties, and Application in Light-Emitting Diodes. *Adv. Mater.* **2022**, 34 (10), 2107105.
- (20) Wu, Y.; Wei, C.; Li, X.; Li, Y.; Qiu, S.; Shen, W.; Cai, B.; Sun, Z.; Yang, D.; Deng, Z.; Zeng, H. In Situ Passivation of PbBr64-Octahedra toward Blue Luminescent CsPbBr3 Nanoplatelets with Near 100% Absolute Quantum Yield. ACS Energy Lett. 2018, 3 (9), 2030–2037.
- (21) Vickers, E. T.; Enlow, E. E.; Delmas, W. G.; DiBenedetto, A. C.; Chowdhury, A. H.; Bahrami, B.; Dreskin, B. W.; Graham, T. A.; Hernandez, I. N.; Carter, S. A.; Ghosh, S.; Qiao, Q.; Zhang, J. Z. Enhancing Charge Carrier Delocalization in Perovskite Quantum Dot Solids with Energetically Aligned Conjugated Capping Ligands. *ACS Energy Lett.* **2020**, *5* (3), 817–825.
- (22) An, H. J.; Kim, Y. C.; Kim, D. H.; Myoung, J.-M. High-Performance Green Light-Emitting Diodes Based on MAPbBr3 with  $\pi$ -Conjugated Ligand. ACS Appl. Mater. Interfaces **2020**, 12 (14), 16726–16735.
- (23) Vickers, E. T.; Graham, T. A.; Chowdhury, A. H.; Bahrami, B.; Dreskin, B. W.; Lindley, S.; Naghadeh, S. B.; Qiao, Q.; Zhang, J. Z. Improving Charge Carrier Delocalization in Perovskite Quantum Dots by Surface Passivation with Conductive Aromatic Ligands. *ACS Energy Lett.* **2018**, 3 (12), 2931–2939.
- (24) Worku, M.; Ben-Akacha, A.; Blessed Shonde, T.; Liu, H.; Ma, B. The Past, Present, and Future of Metal Halide Perovskite Light-Emitting Diodes. *Small Science* **2021**, *1* (8), 2000072.
- (25) Liu, H.; Shonde, T. B.; Gonzalez, F.; Olasupo, O. J.; Lee, S.; Luong, D.; Lin, X.; Vellore Winfred, J. S. R.; Lochner, E.; Fatima, I.; Hanson, K.; Ma, B. Efficient Red Light Emitting Diodes Based on a Zero-Dimensional Organic Antimony Halide Hybrid. *Adv. Mater.* **2023**, 35 (9), 2209417.
- (26) Xu, L.-J.; Worku, M.; He, Q.; Lin, H.; Zhou, C.; Chen, B.; Lin, X.; Xin, Y.; Ma, B. Ligand-Mediated Release of Halides for Color

- Tuning of Perovskite Nanocrystals with Enhanced Stability. J. Phys. Chem. Lett. 2019, 10 (19), 5836–5840.
- (27) Shamsi, J.; Kubicki, D.; Anaya, M.; Liu, Y.; Ji, K.; Frohna, K.; Grey, C. P.; Friend, R. H.; Stranks, S. D. Stable Hexylphosphonate-Capped Blue-Emitting Quantum-Confined CsPbBr3 Nanoplatelets. *ACS Energy Lett.* **2020**, *5* (6), 1900–1907.
- (28) Shamsi, J.; Rastogi, P.; Caligiuri, V.; Abdelhady, A. L.; Spirito, D.; Manna, L.; Krahne, R. Bright-Emitting Perovskite Films by Large-Scale Synthesis and Photoinduced Solid-State Transformation of CsPbBr3 Nanoplatelets. ACS Nano 2017, 11 (10), 10206–10213.
- (29) Shamsi, J.; Dang, Z.; Bianchini, P.; Canale, C.; Di Stasio, F.; Brescia, R.; Prato, M.; Manna, L. Colloidal Synthesis of Quantum Confined Single Crystal CsPbBr3 Nanosheets with Lateral Size Control up to the Micrometer Range. *J. Am. Chem. Soc.* **2016**, *138* (23), 7240–7243.
- (30) Yang, S.; Chen, S.; Mosconi, E.; Fang, Y.; Xiao, X.; Wang, C.; Zhou, Y.; Yu, Z.; Zhao, J.; Gao, Y.; De Angelis, F.; Huang, J. Stabilizing Halide Perovskite Surfaces for Solar Cell Operation with Wide-Bandgap Lead Oxysalts. *Science* **2019**, *365* (6452), 473–478.
- (31) Wu, Y.; Wei, C.; Li, X.; Li, Y.; Qiu, S.; Shen, W.; Cai, B.; Sun, Z.; Yang, D.; Deng, Z.; Zeng, H. In Situ Passivation of PbBr64-Octahedra toward Blue Luminescent CsPbBr3 Nanoplatelets with Near 100% Absolute Quantum Yield. ACS Energy Lett. 2018, 3 (9), 2030–2037.
- (32) Scrocco, M. X-Ray Photoemission Spectra of Pb(II) Halides: A Study of the Satellites on the Core and Valence Bands. *Phys. Rev. B* **1982**, 25 (3), 1535–1540.
- (33) Liu, H.; Worku, M.; Mondal, A.; Shonde, T. B.; Chaaban, M.; Ben-Akacha, A.; Lee, S.; Gonzalez, F.; Olasupo, O.; Lin, X.; Vellore Winfred, J. S. R.; Xin, Y.; Lochner, E.; Ma, B. Efficient and Stable Blue Light Emitting Diodes Based on CsPbBr<sub>3</sub> Nanoplatelets with Surface Passivation by a Multifunctional Organic Sulfate. *Adv. Energy Mater.* 2023, 13 (33), 2201605.
- (34) Nenon, D. P.; Pressler, K.; Kang, J.; Koscher, B. A.; Olshansky, J. H.; Osowiecki, W. T.; Koc, M. A.; Wang, L.-W.; Alivisatos, A. P. Design Principles for Trap-Free CsPbX3 Nanocrystals: Enumerating and Eliminating Surface Halide Vacancies with Softer Lewis Bases. *J. Am. Chem. Soc.* **2018**, *140* (50), 17760–17772.
- (35) Zeng, Q.; Du, Y.; Jiang, J.; Yu, Q.; Li, Y. Revealing the Aging Effect of Metal-Oleate Precursors on the Preparation of Highly Luminescent CsPbBr3 Nanoplatelets. J. Phys. Chem. Lett. 2021, 12 (10), 2668–2675.
- (36) Wang, Y.-K.; Ma, D.; Yuan, F.; Singh, K.; Pina, J. M.; Johnston, A.; Dong, Y.; Zhou, C.; Chen, B.; Sun, B.; Ebe, H.; Fan, J.; Sun, M.-J.; Gao, Y.; Lu, Z.-H.; Voznyy, O.; Liao, L.-S.; Sargent, E. H. Chelating-Agent-Assisted Control of CsPbBr3 Quantum Well Growth Enables Stable Blue Perovskite Emitters. *Nat. Commun.* **2020**, *11* (1), 3674.
- (37) Yang, F.; Chen, H.; Zhang, R.; Liu, X.; Zhang, W.; Zhang, J.; Gao, F.; Wang, L. Efficient and Spectrally Stable Blue Perovskite Light-Emitting Diodes Based on Potassium Passivated Nanocrystals. *Adv. Funct. Mater.* **2020**, *30* (10), 1908760.
- (38) Hoye, R. L. Z.; Lai, M.-L.; Anaya, M.; Tong, Y.; Gałkowski, K.; Doherty, T.; Li, W.; Huq, T. N.; Mackowski, S.; Polavarapu, L.; Feldmann, J.; MacManus-Driscoll, J. L.; Friend, R. H.; Urban, A. S.; Stranks, S. D. Identifying and Reducing Interfacial Losses to Enhance Color-Pure Electroluminescence in Blue-Emitting Perovskite Nanoplatelet Light-Emitting Diodes. ACS Energy Lett. 2019, 4 (5), 1181–1188.